Numerically Closing the Loop of the Adaptive Optics Sensor: the Validation of the COMSOL Multiphysics® Simulation

C. Del Vecchio*,[1], R. Briguglio[1], M. Xompero[1], A. Riccardi[1]
[1]INAF-OAA
*L. Enrico Fermi 5 I-50125 Firenze, Italy, cdelvecchio@arcetri.astro.it

Abstract:

As any other modelling of a physical behavior, the numerical simulation of the mechanical response of an adaptive secondary mirror requires that the results match the experimental data. Achieving such an agreement, recently demonstrated for the actuator forces of the LBT and VLT Deformable Mirrors, also for the shell displacements makes the numerical simulation results a self-consistent set of data on which the control commands may rely on. Moreover, thoroughly reliable modelling avoids to set up the complex optical measuring equipment required by the convex shells and complicated analyses at the mirror inner and outer edges. Finally, accurate numerical data make the calibration easier. For all these reasons, the accuracy of the numerical results is of vital importance. Therefore, the methodology of the comparison with the experimental data must be properly selected.

The feedback signal of the actuator of the Adaptive Optics control system is provided by a capacitive sensor - the displacements is proportional to the capacitance variation. The experimental data are supplied by means of an interferometer as deformation maps. The substantial difference between the model and the physical system is that in the latter the displacements are measured on the annular areas of the capacitive sensors, co-axial with the magnetic force vector, while in the model the displacements are measured directly on the magnet locations. The closed loop ensures that the applied command is equal to the measured position, read on the above mentioned surface. As the system and the model read at different locations, the displacements are obviously different. The implementation of the actual reading on the model is computational overwhelming, so that we identify a matching strategy to transform the model output into data compatible with the actual measures.

After a discussion about the methods adopted to collect the measurement data, this paper shows the numerical procedures selected to run the simulations. Specifically, two key points are emphasized. Firstly, the method chosen to approximate the evaluation of the capacitance variation by computing the displacements along a circumference: the effectiveness of the method is demonstrated by a model refinement. Secondly, the shell mesh strategy which provides a relevant reduction of the computational time: a proper, unusual mesh allows an enough accuracy with a relatively small number of elements. Finally, the correlation of the experimental data and the numerical results is demonstrated. In particular, the comparison of the measurement fitting and of the numerical result fitting are discussed, in order to define the calibration procedure.

As a results, closing the loop without any optical measure is now suitable because of the results of the Comsol computations along with the pyramid wavefront sensor acquisitions.

The methods disclosed in this paper demonstrate that Comsol is fully capable to replicate the measures, even the delicate gauges provided by the capacitive sensors. Properly implementing some computational algorithms in the Structural Mechanics Module and carefully meshing the shell domain allows to defines with enough precision the full set of data required by a completely numeric, highly accurate control system.

Keywords: Adaptive Optics, Optomechanics, Influence Function, FEA

1 Introduction

The matching of the experimental data with the numerical results has been recently demonstrated for the Deformable Mirrors (DM) actuator forces of the Large Binocular Telescope (LBT) and the Very Large Telescope (VLT), as discussed in [2] and [3]. In that paper the measured local mirror stiffness was successfully compared with the numerical results. We extend that approach to the comparison of the whole DM displacements. The goal is to improve the accuracy of the numerical simulations. In fact, reliable modelling avoids to set up the complex optical measuring equipment required by the convex shells and complicated analyses at the mirror inner and outer edges, and allows easier calibrations. Even an ideal, error-free numerical model gives results that are not directly comparable with the experimental data. Consequently, a proper comparison strategy must be identified, in order to avoid systematic errors.

Because of the VLT DM is larger and more optically complex than the LBT one, only the former is treated in this paper — refer to [2] for the overall approach. In Sec. 2 we describe the conceptual differences between the numerical model and the actual system. In Sec. 3 we discuss the model updates and modifications taking into account the mentioned differences. Finally, in Sec. 5 we compare the results of the updated model with the interferometric data described in Sec. 4.

2 Images vs simulations

The key data requested for the optical calibration of a DM are its set of IFs *Influence Functions* (IF). The mirror IF are obtained by poking a single actuator i, out of N, by an arbitrary amount, while keeping the remaining $N - i$ actuators at zero displacement; the mirror image captured by an interferometer is the IF corresponding to actuator i. The displacement is generated by a voice coil driver pushing (or pulling) a magnet glued on the glass. The actuator motion is performed in the physical system in *close loop*; the position reading is provided by a *capacitive sensor* (*capsens*), a metallic annular area acting as a capacitor armature (the other being the thin shell itself), located coaxially with each magnet axis, as shown in Fig. 1. The capacitance value averaged on the *capsens* area is then converted into actuator positions. The close loop mechanism guarantees that the actuator is moved until its position (read by the *capsens*) equals the applied command: for an IF such reading is systematically lower than the magnet one, as the IF is a bell-shaped deformation peaked on the magnet.

The strongest conceptual difference between the FEM and the actual system lies in the displacement reading mechanism. Averaging on the *capsens* area is computationally overwhelming in the numerical model: the displacement is therefore measured at a single point, the location of the magnet. The magnetic force is however applied at the same points in both the model and the system, i.e. on the magnet axes: the magnet displacements may be considered as a vector basis of the displacement space, i.e. each displacement field may be expressed as a linear combination of the magnet motions. Therefore, the real IF deformation field corresponds to a different actuation command in the model. It follows that it is possible to transform (by means of a suitable operator) the simulated data, measured on the magnets, into the experimental ones, where the displacement measurements are taken at the *capsens* locations.

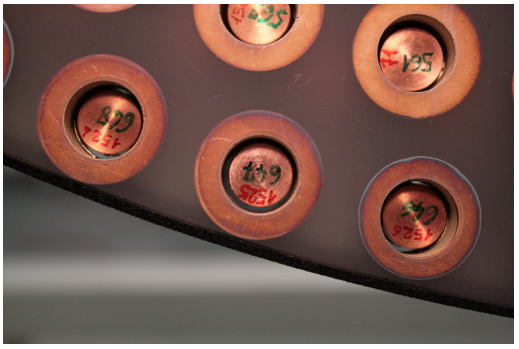

Figure 1: Bottom view of the *capsens* armatures along with their magnets.

3 The numerical approach

Because of the differences described in Sec. 2, the FEM requires to be properly updated, because additional output is needed in the *capsens* areas, where the displacement is actually read. In order to reduce the

output data without any loss in accuracy, we investigate the *capsens* area response as the displacement on a circumference of suitable radius. In particular, the circumferences coaxial with the actuator axes — along with the shell displacements — are added to the geometry FEM and the circles bounded by such circumferences are meshed with a specific method. The radius of the above mentioned circumferences is chosen according to the method in Sec. 3.1. The mesh procedure which provides a relevant reduction of the computational time, without loosing the computational accuracy, is described in Sec. 3.2.

The whole numerical procedure is carried out by means of two Comsol/Matlab scripts — the first one produces the geometry starting from the opto-mechanical data of the DM, the second one creates the model — and a function which computes the IFs iteratively solving and post-processing the model.

3.1 Approximating the capsens signal

We can define the capacitance of the capacitive sensor as

$$C = \int_0^{2\pi} \int_{r_i}^{r_o} \frac{\varepsilon}{z(r,\theta)} r dr d\theta = \frac{\varepsilon A}{z^\star} \qquad (1)$$

where r_o and r_i are the outer and inner radii of the fixed armature of the capacitor, respectively, $A = \pi(r_o^2 - r_i^2)$ is its surface, $\varepsilon = \varepsilon_r \varepsilon_0$ is the product of the dielectric constant of the air times the electric constant, $z(r,\theta)$ is distance between the reference body and the DM, which is, in the most general case, a function of r and θ, and $z^\star$ is the distance resulting from

$$\frac{1}{z^\star} = \frac{1}{A} \int_0^{2\pi} \int_{r_i}^{r_o} \frac{1}{z(r,\theta)} r dr d\theta \qquad (2)$$

Approximating $1/z = f(r,\theta)$ in Eq. 2 with the Taylor series around the expansion point $r^\star$, and omitting terms of higher order than the 4th degree gives, for any θ

$$\frac{1}{z} \approx \frac{1}{z(r^\star,\theta)} + \frac{\partial}{\partial r}\left(\frac{1}{z}\right)\Big|_{r^\star,\theta} (r - r^\star) + \frac{1}{2}\frac{\partial^2}{\partial r^2}\left(\frac{1}{z}\right)\Big|_{r^\star,\theta} (r - r^\star)^2 \qquad (3)$$

Computing the partial derivatives, Eq. 3 gives

$$\frac{1}{z} \approx \alpha - \beta(r - r^\star) + \gamma(r - r^\star)^2 \qquad (4)$$

where $\alpha = \frac{1}{z(r^\star,\theta)}$, $\beta = \frac{\partial z}{\partial r}\frac{1}{z^2}\Big|_{r^\star,\theta}$, and $\gamma = \frac{1}{2z^3}\left(2\left(\frac{\partial z}{\partial r}\right)^2 - z\frac{\partial^2 z}{\partial r^2}\right)\Big|_{r^\star,\theta}$. Substituting the approximation of $\frac{1}{z}$ given by Eq. 4 in Eq. 2 gives

$$\begin{aligned}\frac{1}{z^\star} \approx\ & \tfrac{2\pi}{A}\alpha\left(r_o^2 - r_i^2\right) + \\ & \tfrac{2\pi}{A}\beta\left(r^\star \tfrac{r_o^2 - r_i^2}{2} - \tfrac{r_o^3 - r_i^3}{3}\right) + \\ & \tfrac{2\pi}{A}\gamma\left(r^{\star 2}\tfrac{r_o^2 - r_i^2}{2} - 2r^\star\tfrac{r_o^3 - r_i^3}{3} + \tfrac{r_o^4 - r_i^4}{4}\right)\end{aligned} \qquad (5)$$

and, as $A = \pi(r_o^2 - r_i^2)$,

$$\begin{aligned}\frac{1}{z^\star} \approx\ & \alpha + \beta r^\star - \frac{2}{3}\beta\left(r_i + \frac{r_o^2}{r_o + r_i}\right) + \\ & \gamma r^{\star 2} - \tfrac{4}{3}\gamma r^\star\left(r_i + \tfrac{r_o^2}{r_o + r_i}\right) + \gamma\tfrac{r_o^2 + r_i^2}{2}\end{aligned} \qquad (6)$$

The value of $r^\star$ able to cancel the coefficient of β in Eq. 6 is given by

$$r^\star = \frac{2}{3}\frac{r_o^2 + r_i^2 + r_o r_i}{r_o + r_i} \qquad (7)$$

while no real value of $r^\star$ makes null the coefficient of γ. As a consequence, when reading the capacitive sensor signal at the radial distance of Eq. 7 we obtain only the second-order errors given by multiplying the value of Eq. 7 by γ in Eq. 6. As $r_o = 8.00\,\text{mm}$ and $r_i = 13.50\,\text{mm}$, Eq. 7 gives $r^\star = 10.98\,\text{mm}$.

3.2 The modelling strategy

Adding to the model geometry the circumference of radius $r^\star$ given in Eq. 7 to the FEM geometries described in [2] produces a very large model, because the regular Comsol meshing methods generate a huge number of elements. Still, adopting the *Delaunay* triangulation method for the *capsens* circles is allows to mesh each one of them with only 22 triangles. The vertexes of such triangles correspond to the the glue points described in [2], the nominal locations of the the actuator axes and 16 equispaced point on the circumferences of radius $r^\star$, so ensuring enough spatial resolution in the *capsens* areas, as shown in Fig. 2. Consequently, with its $\approx 916,000$ degrees of freedom, we obtain

a computational handy, compact, and easy-to-run Comsol model. The simulation results are summarized in Fig. 3 for the VLT DM, where the RMS, the standard deviation of the displacements of the circumferences of radius $r^\star$ given in Eq. 7 are plotted along with their ratios at the nominal locations of the actuators. With the obvious exception of the outer and inner rings, the VLT DM exhibits a typical value of such ratios of $\approx 1\%$.

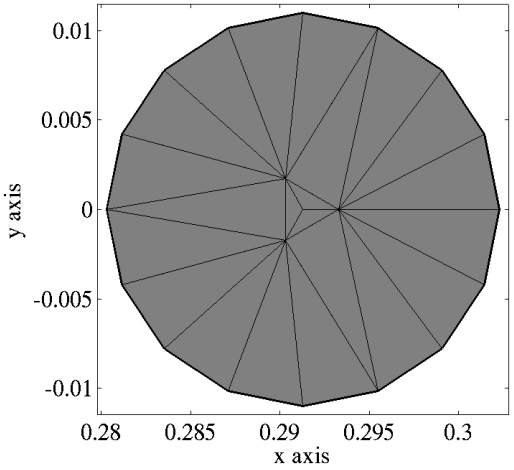

Figure 2: The mesh of the *capsens* area. See the text for a discussion.

The approximation described in Sec. 3.1 is verified by adding the model geometry the two circumferences of radii r_i and r_o at two actuator locations — one on the inner ring and one on a ring roughly halfway between the outer and the inner DM edges —, in order to increase the computational accuracy. The displacement maps of these two annular areas, computed with the above mentioned refined model, are given in Fig. 4. Computing the capacitance difference by numerically computing the surface integral of the displacements shown in Fig. 4 gives values lower by 3.5% and 1%, respectively, than the values given by multiplying the *capsens* areas by the mean displacement of the circumference of radius $r^\star$ for the VLT DM — a good verification of the accuracy of the $r^\star$ defined in Eq. 7. Fig. 5 shows the displacements of the capsens circumferences of radius $r^\star$ of the actuators chosen in Fig. 4 along with their neighbors.

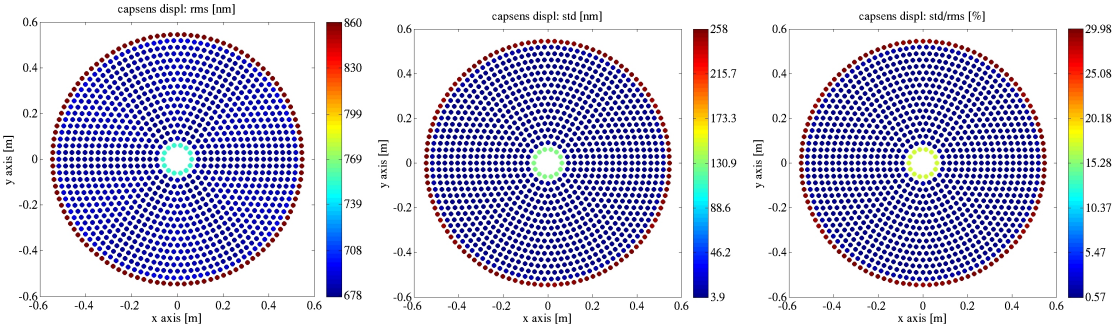

Figure 3: The VLT *capsens* displacements: RMS (left), standard deviation (center) and their ratios (right). See the text for a discussion.

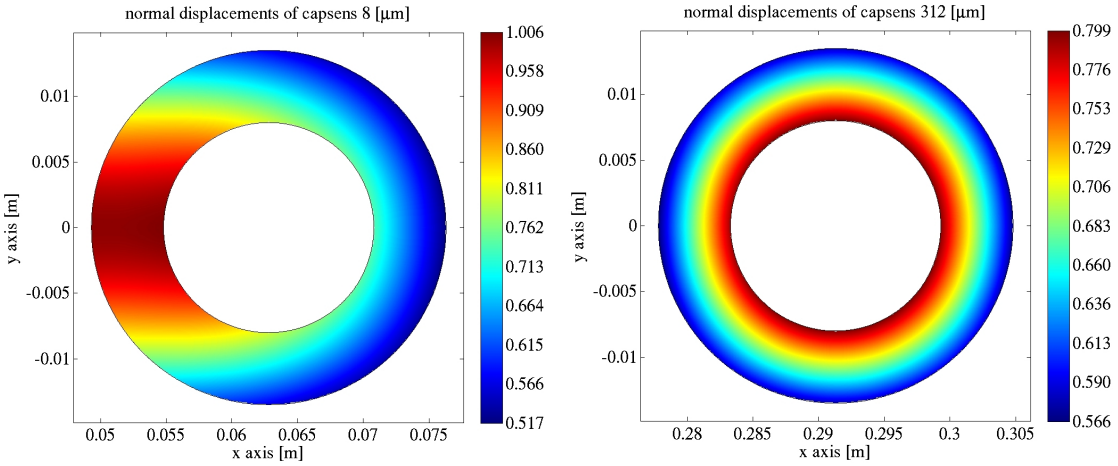

Figure 4: The *capsens* displacements: VLT actuators # 8 @ (0.063,0) (left) and # 312 @ (0.291,0) (right).

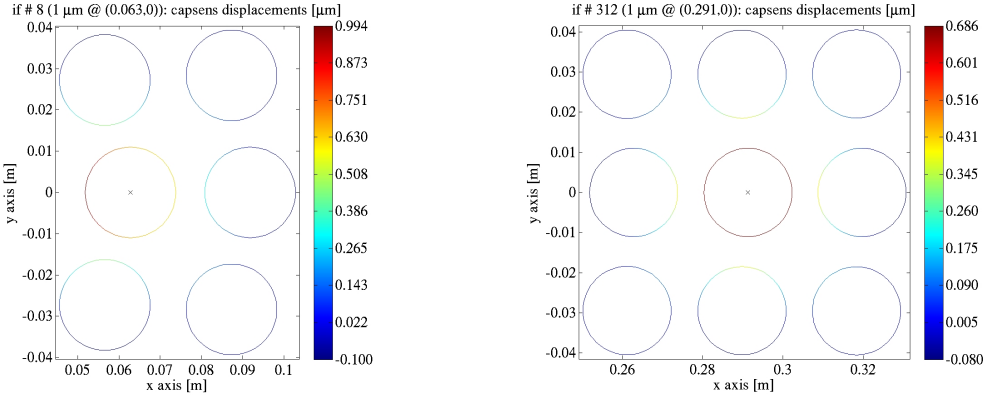

Figure 5: VLT capsens displacements closest to the actuators # 8 @ (0.063,0) (left) and # 312 @ (0.291,0) (right).

4 Interferometric data

The experimental influence function (IF), defined in [2], data consist of image data sets captured by an interferometer, which provides a deformation map of the mirror. The IF data associated with an actuator are collected according to the following procedure, discussed in [1]:

1. a displacement $+c$ is applied to the ith actuator, while the others are constrained at zero;
2. an image w_1 is captured;
3. a displacement $-c$ is applied to the ith actuator, while the others are constrained at zero;
4. an image w_2 is captured;
5. these steps are repeated N times, obtaining $2N$ frames;
6. a resulting image w_m is computed as

$$w_m = \frac{1}{N} \sum_{i=1}^{N} \frac{(w_{i1} - w_{i2})}{2c}$$

This procedure is iterated for all the actuators; the frame rate is 25 Hz, in order to freeze the convection noise; each w_m frame is then corrected for tip-tilt and defocus (the component not filtered out by the differential algorithm); the piston is adjusted so that the mean value of w_m is zero after masking the IF peak; w_m is finally normalized to unitary maximum value. The image noise is given by the convection residuals, computed

as the RMS of the images after masking out the actuated region (a circular area of diameter greater than five times the inter-actuator distance). Its value is .014, to be compared with the unitary IF peak value.

5 Data matching

5.1 Fea data manipulation

According to the method defined in Sec. 2, we need to make the FEM data consistent with the experimental ones. We create a matrix $\mathbf{M}$ to transform the model IF data $\mathbf{F_m}$ (actuator displaced at the magnet locations) into $\mathbf{F_c}$ images (actuator displaced at the capacitive sensor ones). $\mathbf{M}$ is a $n_{act} \times n_{act}$ matrix such that its (i, j) element is the value of $\mathbf{F_m}(i, j)$ (ith IF, jth actuator) averaged over the capacitive sensor ring as mapped on the $\mathbf{F_m}$ image. As a result, $\mathbf{F_c} = \mathbf{M}^{-1}\mathbf{F_m}$, where $\mathbf{M}^{-1}$ is the inverse of $\mathbf{M}$. Each $\mathbf{F_c}$ image is at the end re-aligned in order to match the interferometer images geometry and normalized to unitary maximum value. As a result, a direct comparison between $\mathbf{F_c}$ and the interferometer images is available. The uncertainties in the identification of the *capsens* areas and in the images alignment are possibly responsible for systematic errors in the analysis of the subtraction residuals.

5.2 Comparison

The above defined $\mathbf{F_c}$ images are subtracted from the experimental data, obtaining a difference map; we consider a 80 by 80 pixels area centered at the VLT DM actuator locations, typically including a grid of 5×5 actuators — the IF is practically flat outside this area. We compute the RMS of the difference for each IF. In Fig. 6 the resulting RMS values are plotted at the nominal actuator locations. The interferometric data are not available close to the inner and outer DM edges as well as in the areas obscured by the spiders; some bad pixels have also been detected. In all these cases, these actuator positions are depicted with black dots.

On 849 actuators out of 1170, the RMS difference ranges from .011 to .043, to be compared with the unitary applied displacement. The maximum values are found close to the edges; ≈60% of the considered amount of actuators exhibits a value $\leqslant .02$ — the experimental data noise is typically .014, as shown in Sec. 4. In Fig. 7 we show the normalized interferometric image (left) of a 80 by 80 pixel portion centered at the VLT actuator # 312 (see Fig. 4), the correspondent matrix $\mathbf{F_c}$, defined in Sec. 5.1 (center), and their difference (right), spanning from $-.089$ to .057. Although the latter shows some residue structures, noticeable at the actuator locations, the global matching is within the experimental noise.

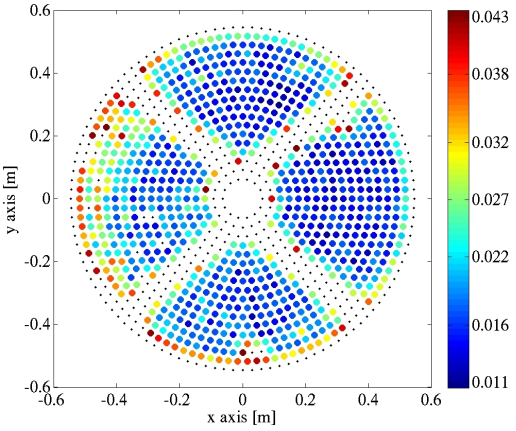

Figure 6: The VLT FEA/image differences. See the text for a discussion.

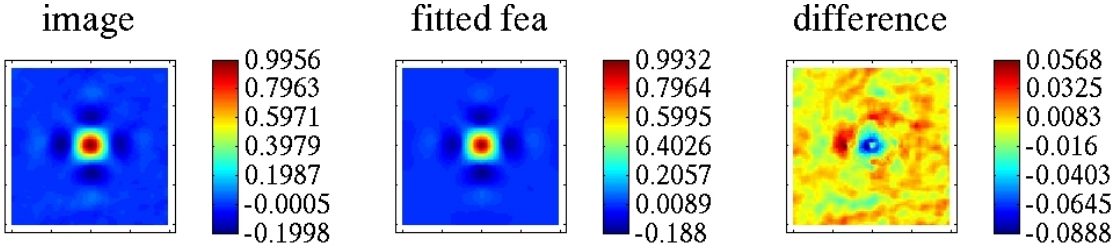

Figure 7: The VLT displacement around actuator # 312. See the text for a discussion.

6 Conclusions

In this paper we characterize a matching strategy able to compare directly the simulated IFs of the VLT DM with the correspondent interferometric data. The entire numerical process is performed by Comsol, computing the simulated IFs via a Matlab function which loads the model generated by two Matlab scripts whose inputs are the optical and mechanical data of the deformable mirror. The difference between the numerical data and the measured ones is within three times the experimental noise, limiting our analysis to the actuators (849 out of 1170) far from the edges. Such a result demonstrates that Comsol is capable to replicate the measures, provided that the simulation is properly set up. Hence, the full set of data required by a completely numeric, highly accurate control system, is now available via the FEA.

Acknowledgments

The optical VLT DM data have been taken in the framework of the Contract for Optical Characterization with the ASSIST optical facility at ESO-Garching of the adaptive mirror unit, as a collaboration between ESO, Microgate S.r.L., ADS S.r.L. and INAF-OAA. The data reduction has been performed with the support of the TECNO-INAF 2010 project.

References

[1] Ciro Del Vecchio, Runa Briguglio, Armando Riccardi, and Marco Xompero, *Analysis of the static deformation matching between numerical and experimental data on the voice-coil actuated deformable mirrors*, Adaptive Optics Systems IV (Enrico Marchetti, Laird M. Close, and Jean-Pierre Véran, eds.), Proc. SPIE, vol. 9148, SPIE, 7 2014.

[2] Ciro Del Vecchio, Runa Briguglio, Marco Xompero, Armando Riccardi, Daniele Gallieni, and Roberto Biasi, *Computing the influence functions of an adaptive optics large deformable mirror: the numerical method and the experimental data*, Comsol Conference, Proc. Comsol, Comsol, 10 2013.

[3] Daniele Gallieni and Roberto Biasi, *The new VLT-DSM M2 unit: construction and electromechanical testing*, Third AO4ELT Conference (Simone Esposito and Luca Fini, eds.), Proc. AO4ELT, AO4ELT, 5 2013.